Received: 12 August 2024 | Revised: 25 December 2024 | Accepted: 27 February 2025

DOI: 10.1002/qj.4975

Quarterly Journal of the Royal Meteorological Society RMetS

RESEARCH ARTICLE

Sensitive areas for target observation associated with meteorological forecasts for dust storm events in the Beijing–Tianjin–Hebei region

Lichao Yang[1] | **Wansuo Duan**[2]

[1]College of Resource Environment and Tourism, Capital Normal University, Beijing, China

[2]State Key Laboratory of Earth System Numerical Modeling and Application, Institute of Atmospheric Physics, Chinese Academy of Sciences, Beijing, China

Correspondence
Wansuo Duan, State Key Laboratory of Earth System Numerical Modeling and Application, Institute of Atmospheric Physics, Chinese Academy of Sciences, Beijing, China.
Email: duanws@lasg.iap.ac.cn

Funding information
National Key Research and Development Program of China, Grant/Award Number: 2023YFC3705501; National Natural Science Foundation of China, Grant/Award Number: 42475064; R&D Program of Beijing Municipal Education Commission, Grant/Award Number: KM202410028014; The numerical simulation was supported by the National Key Scientific and Technological Infrastructure project "Earth System Numerical Simulation Facility" (EarthLab)

Abstract

Accurate meteorological forecasts from the surface to troposphere layers are crucial for dust storm predictions, as even small uncertainties in meteorological conditions can influence the transportation of dust particles, thereby significantly affecting dust storm forecasts. Typically, a greater quantity and higher quality of meteorological observations result in more accurate meteorological outcomes. However, meteorological stations, especially the stations which monitor tropospheric meteorological variables, are sparsely distributed and may not be sufficient for high-quality meteorological forecasts. To address this shortfall, this study investigates the sensitive areas for target observation to enhance meteorological forecasts for dust storm events that struck the Beijing–Tianjin–Hebei (BTH) area from 2021 to 2023, using the Conditional Nonlinear Optimal Perturbation (CNOP) method, which fully considers the impact of nonlinearity. For comparison, the First Singular Vector (FSV) method, which is widely used in operational target observation field campaigns, is also employed to identify the sensitive areas. Results show that although the sensitive areas identified by the two methods are both distributed in the northwest direction of the BTH region, the FSV-based sensitive areas are much closer to the BTH region. By conducting observing system experiments for each dust storm event, we verified numerically and explained physically the advantages of CNOP in determining the sensitive areas in target observation. The result highlights the importance of considering nonlinearity when identifying the sensitive areas for target observation and may provide a theoretical foundation for establishing upper-air radiosonde sites or planning practical field observation campaigns.

KEYWORDS

Conditional Nonlinear Optimal Perturbation, dust storm, target observation

1 | INTRODUCTION

Dust storms are a frequent meteorological hazard in East Asia during the spring season. Despite China having made notable achievements in addressing desertification in past decades (Zhang & Huisingh, 2018), severe dust storms still occasionally occur in northern China due to the transboundary dust and sand particles, posing a serious threat to Chinese ecological security (Vova et al., 2015; Chen et al., 2023). Particularly since the 2020s, northern China

has increasingly suffered from several severe dust storm events. The super dust storm on 15 March 2021, regarded as the most severe dust storm event in the past decade, has affected an area covering approximately 450,000 square kilometers and resulted in economic losses of over 30 million RMB (Yin et al., 2022). In the spring of 2023, China experienced a total of 12 dust storm events, the highest frequency recorded in nearly a decade (Chen et al., 2023). The severe and frequent dust storm events not only cause environmental pollution and affect people's health, but sand and dust particles can also change the radiation balance of the earth–atmosphere system, thereby significantly impacting the weather systems and long-term climate change (Feng et al., 2023; Shao et al., 2013). Due to the significant impacts of dust storm events on human society and the earth–atmosphere system, the accurate forecast of dust storms has always been a focal and hot research topic (Chen et al., 2024).

In contrast to statistical forecast models (i.e., machine-learning-based models), which primarily rely on establishing statistical relationship between the meteorological variables and dust concentrations, numerical forecast models can simulate the emission, transportation and deposition of dust particles, thereby being the primary tool for forecasting the dust storms in both scientific research and operational forecasts (Bao et al., 2019; Kaimian et al., 2019; Gholami et al., 2020; Gong & Zhang, 2008). Starting from the 1970s, many efforts have been made to improve the skills of numerical forecasting of dust storms, including establishing sandstorm prediction systems, developing the parameterization of dust emission flux and assimilating multiple sources of observations (Gong & Zhang, 2008; Zhang & Li, 2014; Zhang, Mu, et al., 2019a, Zhang, Sharratt, et al., 2019b). However, due to the multiscale nature of the governing meteorological dynamics and the complex coupling between the dust particles and meteorological variables, the current numerical forecasting capability for sandstorms is still insufficient and contains large uncertainties (Chen et al., 2024; Knippertz & Todd, 2012). The Weather Research and Forecasting (WRF) model coupled with chemistry (WRF-Chem) model, which is a coupled model and widely used in dust forecasts, struggles to capture the dust observations during dust events. Specifically, under dusty conditions characterized by aerosol optical depths (AODs) greater than one, the correlation between simulated and observed AOD values at the Mezaira station, situated in a major dust source region in Saudi Arabia, is only 0.42 (Ukhov et al., 2021). Evaluations of the European Centre for Medium-Range Weather Forecasts (ECMWF) Integrated Forecasting System (IFS), which is the operational forecast system in ECMWF, also show that even though it can well forecast the long-range transport regional dust event (appearance, dissolution), the forecast peak dust concentrations remain underestimated (Chan et al., 2018). Using the Chinese Unified Atmospheric Chemistry Environment for Dust forecasting system (CUACE/Dust), which is an integrated system for operational dust forecasting in Asia, the threat score of 2006 spring dust storms was 0.31, 0.23 and 0.21 for the 24-, 48- and 72-hour forecasts, respectively (Gong & Zhang, 2008). Despite assimilating the Fengyun-3 aerosol optical depth data, the threat score only reaches 0.2 for events with a PM_{10} threshold of 200 $\mu g \cdot m^{-3}$ (Bao et al., 2019). Recently, Chen et al. (2023) reviewed the forecasting capability for transboundary dust events and found that the accuracy rate is only 30%–51%, while false alarms peak at 49%–70%. Thus, the capability of numerical forecasts of dust storm events remains limited and enhancing their numerical forecast skills is still urgently needed.

Dust storms typically occur under weather conditions characterized by unstable atmospheric stratification and strong surface winds (Qian et al., 2006). Moreover, the horizontal and vertical transport of sand particles largely depends on mid-to-lower tropospheric meteorological factors such as wind shear, temperature, and precipitation (Gui et al., 2023; Lin et al., 2009). Thus, accurate meteorological forecasts are crucial for acquiring high forecast levels of dust storms. It has been confirmed numerically by many previous studies that the meteorological forecasts play significant roles in predicting the dust storms. During the dust storm event occurring in North China from 27 to 30 March 2015, the operation departments underestimated both the intensity and coverage area of the dust storm. By analyzing the forecast results from ECMWF and CUACE/Dust, An et al. (2018) showed that such underestimation is mainly attributed to rapid changes of the weather situation so that the transport of dust particles from south to north was not accurately predicted. Duan et al. (2016) studied several dust storm forecast results with the Global/Regional Assimilation and Prediction Enhanced System (GRAPES_SDM) and found the higher false rates are primarily attributable to the forecast errors in near-surface temperature and wind speed. To quantify the uncertainties of meteorological fields on dust storm forecast, Lin et al. (2009) designed a few sensitivity experiments and showed that for a typical dust storm event that affected Beijing city, when the mid-to-lower tropospheric wind speed increases by only 20%, the root-mean-squared error (RMSE) of highest PM_{10} concentration forecast increases by nearly 1000 $\mu g \cdot m^{-3}$; while when the surface wind speed decreases by 30%, the RMSE of PM_{10} concentration decreases by 62%. The tropospheric wind fields guide the transportation of dust particles, while the surface wind field directly impacts the calculation of friction velocity and then, influences dry deposition velocity and dust

concentration (Ganor et al., 2010; Sarafian et al., 2023). Therefore, to improve the forecast skills of dust storms, it is crucial to provide high-quality meteorological forecasts from surface to tropospheric atmospheric layers during dust events.

Identifying the main sources of forecast uncertainties and reducing the uncertainties are the fundamental ways for acquiring high-quality meteorological forecasts. It is widely accepted that the meteorological forecast errors primarily stem from inaccuracies in the meteorological initial conditions (Leith, 1974; Lorenz, 1963, 1975; Slingo & Palmer, 2011; Toth & Kalnay, 1997). So, it is inferred the meteorological initial errors will lead to significant meteorological forecasts errors and then influence the dust storm forecast accuracy. With the application of the WRF-Chem ensemble forecast system, Bei et al. (2017) demonstrated that the meteorological initial conditions could lead to a rather large ensemble spread for simulations of the aerosol constituent, and the ratio of ensemble spread to the ensemble mean may exceed 50%. Similar results can also be obtained by applying other dust ensemble forecast systems (Lin et al., 2008; Zhu et al., 2009). Thus, accurate meteorological initial states are of vital importance for precise dust concentration forecasts. Data assimilation is a common strategy used to reduce forecast errors induced by initial errors (Bauer et al., 2015; Talagrand, 1997). It integrates real-world measurements with numerical model outputs and their associated error statistics to produce a more accurate representation of the initial state (Talagrand, 1997). To get reliable data assimilation, sufficient and effective observations are essential. Although thousands of ground meteorological station have been constructed in the past few years and assimilating them may benefit the dust storm forecast, the stations are mainly distributed in densely populated areas, and these surface observation data are insufficient to produce accurate dust storm forecasts. As Lin et al. (2009) demonstrated, tropospheric meteorological variables will further influence the transport of dust particles and thus, significantly impact the accuracy of dust storm forecasts. Tropospheric meteorological observations are usually obtained from upper-air radiosonde sites (https://www.weather.gov/upperair/). However, the constructed upper-air radiosonde sites are sparsely distributed and may not be enough to provide a high quality of initial conditions (Mee Kim et al., 2013). Even though the satellite observations may be sufficient to provide an accurate meteorological initial field, the assimilation of more observations may not necessarily enhance forecast accuracy (Zhang, Mu, et al., 2019a). To significantly improve the forecast skills, it is crucial to determine observations on which areas should be preferentially assimilated. Assimilating observations from areas with high sensitivity will greatly enhance forecast skills. Conversely, assimilating observations from areas with low sensitivity will result in minimal or even negative improvements (Yang et al., 2022; Yu et al., 2012). Therefore, identifying the areas with high sensitivity to meteorological forecasts of dust storm events, and assimilating additional observations on such areas will benefit the meteorological forecasts, and then the dust storm forecasts.

Such an idea belongs to the study of "target observation," or "adaptive observation," which means that assimilating additional observations in specific areas (i.e., sensitive areas) can significantly improve the forecast skills in the focused area (verification area) at a future time (verification time), compared to other areas (Majumdar, 2016; Mu et al., 2015; Snyder, 1996). In 1997, the multinational Fronts and Atlantic Storm Track Experiment (FASTEX) field campaign was the first to introduce the target observation technique to identify the sensitive areas for realistic forecasts of frontal cyclones over Europe (Joly et al., 1997). The success of FASTEX, with forecast improvements of 10%–15% as a result of target observation, motivated the international Atmospheric Science Program "Observing System Research and Predictability Experiment" from 2005 to 2014 (THORPEX), aiming at improving 1–4-day forecasts of phenomena such as winter storms, tropical cyclones, and precipitation (THORPEX; Majumdar et al., 2011). Meanwhile, theoretical studies associated with target observation have increased such developing methods for identifying the most sensitive areas. Owing to its successful application in both practical field observation experiments and theoretical research related to various weather and climate events, including typhoons, El Niño–Southern Oscillation (ENSO) and mesoscale eddies, target observation has now emerged as an effective strategy for enhancing the accuracy of numerical forecasts (Chen et al., 2018; Duan et al., 2023; Feng et al., 2022; Jiang et al., 2022; Qin et al., 2023). Actually, the target observation strategy has been applied to improve the meteorological forecasts for dust storm events. To enhance the meteorological forecast accuracy for dust events in Korea, using the adjoint method Mee Kim et al. (2008, 2013) identified the sensitive areas of meteorological fields for dust events. Through observing system simulation experiments (OSSE), they demonstrated that adding few observations in the sensitive areas could yield greater enhancements in meteorological forecast performance compared to adding observations randomly. To address the issue of insufficient tropospheric meteorological observations for Korean dust forecasts, on the basis of the constructed upper-air radiosonde sites, Yang et al. (2014) designed an additional upper-air radiosonde observation network based on the characteristics of the sensitive areas. Later, by applying the more advanced First

Singular Vector (FSV) approach, Goris and Elbern (2015) also arrived at similar conclusions, that assimilating fewer observations on the sensitive areas could largely improve the forecast skills of air polluted events.

However, the approaches they used to identify the sensitive areas, whether adjoint sensitivity or FSV, are developed assuming that initial errors evolve linearly within a nonlinear model. This assumption does not fully reflect the complexities of the real atmosphere. Although assimilating the observations on the sensitive areas determined using linear methods has positive benefits for forecast accuracy, the real atmospheric processes are highly nonlinear and the sensitive areas determined by the linear methods may deviate from the real sensitive areas, significantly reducing the effectiveness of target observations in meteorological forecasts which are affected by strongly nonlinear process. To address the limitation of linear methods, Mu et al. (2003) proposed the Conditional Nonlinear Optimal Perturbation (CNOP) method, which can fully consider the nonlinear impact of the initial error evolution. The CNOP represents the initial perturbation that causes the largest forecast error, offering the potential to identify more effective sensitive areas. Recently, the advantage of CNOP in identifying the sensitive areas has been demonstrated by both theoretical studies and practical observation tasks related to tropical cyclones, ENSO and mesoscale eddies (Duan et al., 2023; Hu & Duan, 2016; Jiang et al., 2022; Qin et al., 2023). Such successful attempts inspire us to investigate the role of nonlinearity in identifying the sensitive areas of meteorological fields for dust storm event forecasts and illustrate the role of target observations in a more realistic way. Then we naturally ask the following questions: how can we use the CNOP method to determine the sensitive areas related to meteorological forecasts for dust storm events? Compared to the traditional FSV method, will assimilating target observations on the CNOP-based sensitive areas lead to greater improvements in forecasting skill? If so, why are the target observations on the CNOP-based sensitive areas more effective in enhancing forecast accuracy?

To address these questions, this study utilizes the CNOP and FSV methods to identify the sensitive areas related to meteorological forecasts for six severe dust storm events that affected the Beijing–Tianjin–Hebei (BTH) region, a major economic and metropolitan area in northern China that has frequently experienced dust storms since the 2020s. Although various methods have been employed before to determine the distributions of sensitive areas, the FSV method is compared here since it is the key method for determining sensitive areas in operational forecasts and practical target observation field campaigns (Parsons, 2017). First, we compare the spatial distributions of sensitive areas determined by the CNOP and FSV methods. Next, to verify the effectiveness of the CNOP method, the improvements in numerical meteorological forecasts achieved by assimilating the same number of observations on the CNOP- and FSV-based sensitive areas, respectively, for each dust storm event are compared. Finally, physical interpretations on why assimilating observations on the CNOP-based sensitive areas lead to higher meteorological forecast skills are presented. Our study may provide a theoretical basis for the deployment of upper-air meteorological detection instruments in field campaigns or the practical establishment of upper-air meteorological sites, thereby enhancing meteorological forecasts and improving dust storm predictions.

The article is arranged as follows: the cases, model and method we used are introduced in Section 2. In Section 3, we identify the sensitive areas of meteorological forecasts for dust storm events using the CNOP and FSV methods, respectively. Subsequently, a comparison of the effectiveness of CNOP and FSV in improving meteorological forecasts for dust storm events through a series of numerical experiments is presented in Section 4. In Section 5, we attempt to provide physical interpretations of why the target observations can lead to higher meteorological forecast skills. Finally, we summarize our study in Section 6.

2 | CASES, MODEL AND METHODS

In the study, the WRF model, along with its adjoint model WRFPLUS, is utilized to compute the CNOP sensitivity of meteorological fields associated with six dust storm events in the BTH region.

2.1 | Cases

From the years 2021 to 2023, six dust events reached the levels of dust storm, significantly impacting the BTH region (Table 1). The maximum PM_{10} concentration ranges from 500 to 1550 $\mu g \cdot m^{-3}$. Particularly, during 21–23 March 2023, the maximum PM_{10} concentration reached 1550 $\mu g \cdot m^{-3}$, the highest level ever recorded in the past 10 years. This study focuses on the meteorological forecasts related to the six dust storms. Since it usually takes 24 hours for dust particles originating from Mongolia (i.e., the southern Gobi region in Mongolia) to be transported to the BTH region we investigated (Piao et al., 2023), the forecast time for each event is defined as the moment when observed PM_{10} concentrations in the BTH region peak, and two forecasts with lead times of 12 and 24 hours are studied, respectively. Consequently, this study analyzes a total of six 12-hour forecasts and six 24-hour forecasts.

TABLE 1 A brief introduction to six dust storm events that impacted the BTH region from 2021 to 2023.

Case no.	Forecast time (UTC time, day month year)	Maximum PM_{10} ($\mu g \cdot m^{-3}$)	12-hr forecast error (wind: $m \cdot s^{-1}$/temp: °C)	24-hr forecast error (wind: $m \cdot s^{-1}$/temp: °C)
1	0600, 15 March 2021	1481.8	6.04/3.31	6.09/3.52
2	0600, 28 March 2021	1244.0	5.07/1.21	5.23/1.39
3	1200, 15 April 2021	629.8	5.56/1.14	6.05/1.18
4	1800, 10 March 2023	561.5	6.69/2.58	6.61/2.34
5	0600, 22 March 2023	1550.8	4.67/2.26	5.04/2.83
6	1800, 10 April 2023	1037.6	5.94/2.60	6.30/2.45

Note: The forecast time and the concentration of the maximum PM_{10} are based on the observations on the BTH region. The 12- and 24-hour forecast errors in wind and temperature fields averaged over the BTH region are listed.

2.2 | Model configuration

We used WRF version 3.6 to generate the meteorological forecast fields. The horizonal model domain covers 119×119 grid points, with a horizonal resolution of 30 km. A vertical configuration with 25 levels, extending up to a top level of 100 hPa, is adopted. The physical parameterizations used in the WRF model contain the Yonsei University planetary boundary layer parameterization scheme, Dudhia shortwave radiation scheme, RRTMG longwave radiation and Lin microphysics scheme (Dudhia, 1989; Hong et al., 2006; Iacono et al., 2008; Lin et al., 1983). The same physical parameterization is also used in its tangent linear model and adjoint model when computing the CNOP and FSV sensitivities.

To obtain the meteorological forecasts, the National Centers for Environmental Prediction (NCEP) GFS forecast dataset is adopted to generate the initial and boundary conditions for WRF simulations. Since it is hard to obtain three-dimensional meteorological observations that accurately describe the true state of the troposphere, the fifth-generation ECMWF reanalysis data (ERA5) are taken as an approximation of real observations. The ERA5 reanalysis is generated by combining large amounts of observations and advanced numerical models and can well describe the real atmospheric variability (Hersbach et al., 2020).

2.3 | Conditional nonlinear optimal perturbation

Assume that a nonlinear model $\boldsymbol{M}$ acts on an n-dimensional initial state vector $\boldsymbol{x_0} \in \boldsymbol{R^n}$, so that $\boldsymbol{x}(t) = \boldsymbol{M}(\boldsymbol{x_0})$, where t is the forecast time, and $\boldsymbol{x}(t)$ is the state vector at forecast time t. If an initial perturbation $\delta \boldsymbol{x}_0$ is added to the initial state, then the final state at forecast time t can be written as $\boldsymbol{x}(t) + \delta \boldsymbol{x}(t) = M(\boldsymbol{x}_0 + \delta \boldsymbol{x}_0)$. The $\delta \boldsymbol{x}(t)$ describes the evolution of initial perturbation $\delta \boldsymbol{x}_0$ relative to the reference state $\boldsymbol{x}(t)$. The CNOP ($\delta \boldsymbol{x}_0^*$) is the initial perturbation satisfying certain constraint and has the largest nonlinear evolution at time t, as shown in Equation (1):

$$J(\delta \boldsymbol{x}_0^*) = \max_{\delta \boldsymbol{x}_0^T C_1 \delta \boldsymbol{x}_0 \le \beta} [M(\boldsymbol{x}_0 + \delta \boldsymbol{x}_0) - M(\boldsymbol{x}_0)]^T C_2 [M(\boldsymbol{x}_0 + \delta \boldsymbol{x}_0) - M(\boldsymbol{x}_0)]. \quad (1)$$

$\delta \boldsymbol{x}_0^T C_1 \delta \boldsymbol{x}_0 \le \beta$ is the initial constraint condition and β is a pre-assigned positive value. C_1 and C_2 are matrices that define the norms of the initial perturbation and its evolution. Obviously, the CNOP denotes the initial perturbation with the potential to generate the largest forecast errors, given certain constraint conditions.

As we mentioned in Section 1, meteorological errors in wind and temperature from surface to middle-tropospheric layers will result in large forecast uncertainties of dust storms. Therefore, in this study, the state vector $\boldsymbol{x}$ consists of zonal (U) and meridional wind (V), temperature (T) and surface pressure (P_s) components. The total dry energy norms from ground to top in the whole model domain (D_1), and from ground to middle-level (i.e., $\sigma = 0.5$) in the verification areas (D_2, BTH region) are used to measure the initial perturbation (Equation 2) and its evolution (Equation 3) respectively.

$$C = \frac{1}{D_1} \int_{D1} \int_0^1 \left[U_0'^2 + V_0'^2 + \frac{c_p}{T_r} T_0'^2 + R_a T_r \left(\frac{P'_{s0}}{p_r} \right)^2 \right] d\sigma dD_1, \quad (2)$$

$$J = \frac{1}{D_2} \int_{D2} \int_0^{0.5} \left[U_t'^2 + V_t'^2 + \frac{c_p}{T_r} T_t'^2 + R_a T_r \left(\frac{P'_{st}}{p_r} \right)^2 \right] d\sigma dD_2. \quad (3)$$

U', V', T' and P'_s are the perturbed variables. C_p(=1005.7 $J \cdot kg^{-1} \cdot K^{-1}$), R_a(=287.04 $J \cdot kg^{-1} \cdot K^{-1}$), T_r(=270 K) and

P_r(=1000 hPa) are physical parameters. Thus, in our study, the CNOP-type initial perturbations, including wind, temperature and pressure variables with a certain constraint condition, will result in the largest meteorological forecast error measured by total dry energy in the BTH region at the forecast time.

After we clarified the optimization problem, the spectral projected gradient 2 (SPG2) algorithm is adopted to compute CNOP (Birgin et al., 2001). The SPG2 algorithm is an optimization method designed for solving a minimum problem of nonlinear function with certain initial condition constraints. Thus, when we compute the CNOP concerned here, we rewrote Equation (1) as Equation (4).

$$J'\left(\delta \boldsymbol{x}_0^*\right) = \min_{\delta \boldsymbol{x}_0^T C_1 \delta \boldsymbol{x}_0 \le \beta} -[M(\boldsymbol{x}_0 + \delta \boldsymbol{x}_0) - M(\boldsymbol{x}_0)]^T C_2[M(\boldsymbol{x}_0 + \delta \boldsymbol{x}_0) - M(\boldsymbol{x}_0)] \tag{4}$$

The SPG2 uses gradient descent combined with a projection step to handle constraints. The specific steps are as follows. First, a first guess of initial perturbation ($\delta \boldsymbol{x}_0^1$) is added to the initial state $\boldsymbol{x_0}$. Then the WRF model is integrated forward, with the initial state $\boldsymbol{x}_0 + \delta \boldsymbol{x}_0^1$. At the forecast time t, we can get the forecast state $M\left(\boldsymbol{x}_0 + \delta \boldsymbol{x}_0^{\boldsymbol{1}}\right)$. By subtracting the reference state $M(\boldsymbol{x_0})$, we can get $J'(\delta \boldsymbol{x}_0^1)$. Then the gradient of $J'(\delta \boldsymbol{x}_0^1)$ with respect to the initial perturbation ($\delta \boldsymbol{x}_0^1$) is calculated, using the adjoint model of WRF. Theoretically, the gradient represents the fastest descending direction of the cost function. In numerical experiments, the gradient keeps a fast-descending direction but is not necessarily the fastest. We still need to update the initial perturbation using the gradient and project the perturbation to satisfy the initial constraint. Then the updated initial perturbation is added to the initial state and the WRF model is forward-integrated again. By iterative forward and backward integration using WRF and its adjoint model governed by SPG2, the initial perturbation is optimized. The algorithm terminates when the convergence criteria are met, and then the optimized initial perturbation, which is CNOP, can be obtained. For more details, please refer to Yang et al. (2023).

2.4 | First singular vector

CNOP is a natural generalization of FSV in nonlinear dynamical regime. To facilitate their comparison, we also briefly introduce the FSV method in this section.

The FSV method, which is the key method in operational forecasts and practical target observation field campaigns, represents the fast-growing perturbation in a linearized model (Parsons, 2017; Peng & Reynolds, 2006). To describe the linear evolution of initial perturbation, the forward-tangent propagator $\boldsymbol{L}$ is used. If there is an initial perturbation ($\delta \boldsymbol{x}_0$) on the initial state, then the evolution of the initial perturbation at forecast time t can be presented as $\delta \boldsymbol{x}_t = \boldsymbol{L}(\delta \boldsymbol{x}_0)$. In that case, the optimization problem defined in Equation (1) can be rewritten via Equation (5).

$$J\left(\delta \boldsymbol{x}_0^L\right) = \max_{\delta \boldsymbol{x}_0^T C_1 \delta \boldsymbol{x}_0 \le \beta} [\boldsymbol{L}(\delta \boldsymbol{x}_0)]^T C_2[\boldsymbol{L}(\delta \boldsymbol{x}_0)] \tag{5}$$

The format of both initial and final perturbations is consistent with those used in the CNOP method. Moreover, the amplitude of the constraint for FSV-type error is the same as that for CNOP.

The computation of FSV is also similar to that of CNOP, with the primary difference being the forward models used for integration in the optimization process. For FSV, the tangent linear model of WRF is employed, whereas the nonlinear WRF model is used for CNOP.

3 | THE SENSITIVE AREAS OF METEOROLOGICAL FIELDS FOR THE DUST STORM EVENTS

In this section, we first show the meteorological forecast errors during the dust storm events, which will influence the transport and deposition of dust particles, thereby the accuracy of dust storm forecast skills. To reduce the meteorological forecast errors, we computed the CNOP- and FSV-type initial errors in the concerned dust storm forecasts. Based on these initial errors, the sensitive areas of meteorological forecasts for each dust storm event are identified, respectively.

3.1 | The meteorological forecast errors of the dust storms

The dust storm events in the BTH region usually occur under the conditions of strong wind and low temperature. In this study, as mentioned in Section 2.1, a total of twelve forecasts at the time when observed PM_{10} concentrations reached their maximum with lead times of 12 and 24 hours are studied. To quantify the meteorological forecast error, we generated the meteorological forecasts by the WRF model initialized by GFS data, which are considered as "control forecast." The ERA5 reanalysis data are taken as the "observation" data (the "truth") since they are created by combining large amounts of observation with the advanced model and have been widely accepted as an approximation of the real atmospheric condition (Hersbach et al., 2020). The discrepancies between

the control forecast and the "truth" are forecast errors. Table 1 summarizes the wind and temperature forecast errors averaged from surface to mid-troposphere level ($P = 500$ hPa) on the BTH region at the forecast time. For the 12-hour forecasts, the average forecast error in wind fields is 5.66 $m \cdot s^{-1}$ and 2.18°C in the temperature field; while for the 24-hour forecasts, the mean error is 5.89 $m \cdot s^{-1}$ in wind fields and 2.29°C in temperature fields. For the event occurring at 1800 10 March 2023, the meteorological forecast errors of wind and temperature can reach 6.61 $m \cdot s^{-1}$ and 2.34°C. According to Lin et al. (2009) and Bei et al. (2017), small uncertainties of wind field may lead to large aerosol concentration forecast errors. Thus, the capability of meteorological forecasts for the dust storm events is limited and efforts are still needed to enhance the meteorological forecast levels.

The target observation strategy aims to enhance forecast accuracy by reducing initial errors in numerical forecasts. As we introduced in Section 2.2, the CNOP represents the initial error that has the largest nonlinear evolution in the focused region at the forecast time. The areas where large CNOP-type errors are concentrated likely contribute most to forecast errors and can therefore be regarded as the sensitive areas for target observation. Preferentially eliminating the initial errors in such sensitive areas by data assimilation could help enhance the forecast skills in the focused region at the forecast time to a large extent. This process is essentially a form of observing-system experiment (OSE, Kalnay, 2002). Thus, in our study, we first computed the CNOP in the control run and identified the sensitive area based on that. The meteorological observations over the sensitive areas are extracted from the ERA5 reanalysis, including wind speed, wind direction, temperature at the surface, 850-, 700-, 500-, 300-, and 200-hPa layers, which are general meteorological variables monitored in the field campaigns. These observations are then assimilated into the control forecast (forecast initialized by GFS data) through the 3DVar assimilation system of WRF, finally obtaining an updated forecast, which is called the assimilation forecast. If the assimilation forecast is much closer to the truth than the control forecast, it indicates that the sensitive areas are effective. Similarly, the FSV-type errors are also computed in the control run and the relevant sensitive areas are identified. Another assimilation forecast can then be generated by assimilating the observations from the FSV-based sensitive areas. If assimilating the same number of observations from the CNOP-based sensitive areas results in higher meteorological forecast skills than assimilating those from the areas identified based on FSV, it indicates that the CNOP-based sensitive areas are more effective in target observations.

3.2 | The sensitive area of meteorological fields for dust storm forecasts determined by CNOP-type errors

In the previous subsection, we showed the meteorological forecast errors for the dust storm predictions. To improve the meteorological forecasts during the Asian dust events, Yang et al. (2014) designed an additional observation network based on the linear method and have shown the effectiveness of additional simulated meteorological observations for improving the meteorological forecast skills through OSSEs. Such a successful attempt inspires us to further adopt the nonlinear CNOP method to determine the sensitive areas for dust storm forecasts and illustrate the role of observations in a more realistic way. It is expected that when the "real" observations are assimilated for the sensitive areas which are determined by fully considering the impacts of nonlinear processes, higher forecasting skills of the meteorological conditions can be obtained.

Now we calculate the CNOP-type errors in each control forecast, as introduced in Section 2.3; in total, twelve CNOP-type errors are obtained. Since in each forecast, the large CNOP components (U, V or T) at different vertical levels may be distributed in different areas (see Figure S1), we refer to Yang et al. (2022) and adopt the vertical integral to evaluate the comprehensive sensitivity of CNOP (Equation 4). The Total Dry Energy norm (TDE) considers all the concerned meteorological variable perturbations and measures the comprehensive initial sensitivities. In this situation, the meteorological forecasts could be sensitive to the areas with larger values of TDE (sensitive areas), and preferentially eliminating the initial errors on such sensitive areas by data assimilation may help enhance meteorological forecast accuracy more effectively than addressing errors in other areas, ultimately improving the dust storm forecast levels.

$$\mathrm{TDE} = \frac{1}{2}\left(U'^2 + V'^2 + \frac{C_p}{T_r} T'^2 + R_a T_r \left(\frac{P'}{P_r} \right)^2 \right). \quad (6)$$

Figure 1 presents the horizonal distribution of the TDE for the 12-hour forecasts in six dust storm events. Even though the specific structures of the sensitive areas are different, five out of six sensitive areas are lying in the region of eastern Mongolia. This implies that the uncertainties of meteorological initial conditions in the eastern part of Mongolia play important roles for the 12-hour meteorological forecasts in the BTH region for most of the concerned dust storm events. In particular, for the case that occurred at 1800 UTC 10 March 2023, besides eastern Mongolia, some regions in the western part of the BTH region, such as central parts of Shanxi Province, also present as sensitive

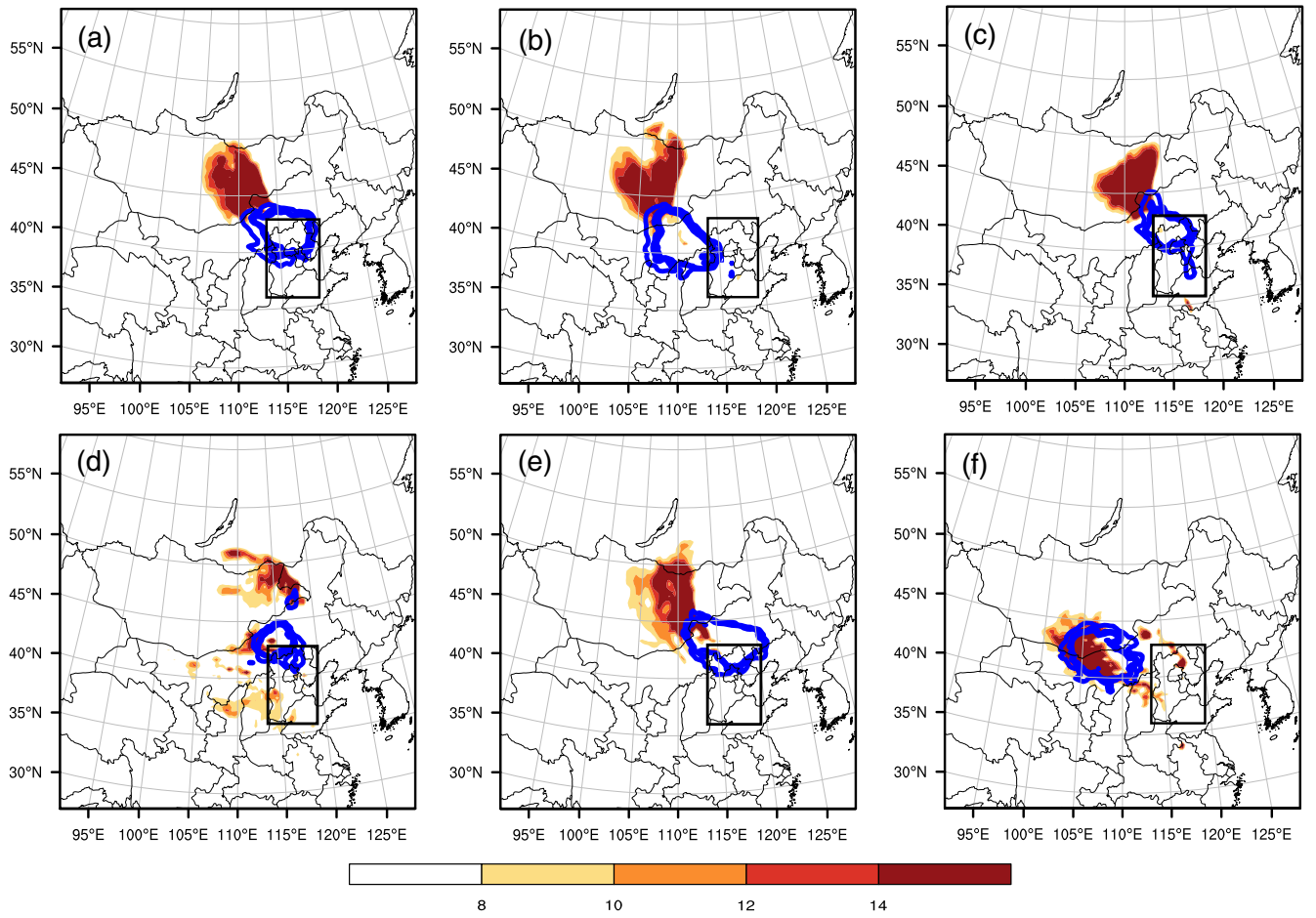

FIGURE 1 The spatial distributions of the TDE (units: $J \cdot kg^{-1}$) values computed from Conditional Nonlinear Optimal Perturbation (CNOP)-type error (shaded) and FSV-type error (contour line in blue) for the 12-hour forecasts in the six dust storm events concerned. (a) The case occurring at 0600 UTC on 15 March 2021; (b) the case occurring at 0600 UTC on 28 March 2021; (c) the case occurring at 1200 UTC on 15 April 2021; (d) the case occurring at 1800 UTC on 10 March 2023; (e) the case occurring at 0600 on 22 March 2023; and (f) the case occurring at 1800 on 10 April 2023. [Colour figure can be viewed at wileyonlinelibrary.com]

areas. For the case that occurred at 1800 UTC on 10 April 2023, the sensitive areas are not located in eastern Mongolia, but are much more western, mostly located in the western Inner Mongolia.

When the lead time increases from 12 to 24 hours, the sensitive areas are more to the northwest of the BTH region (Figure 2). Even though the specific structure of sensitive areas depends on each case, five out of the six sensitive areas are mostly located around the northern part of Mongolia, closer to the southern part of Lake Baikal. This indicates that the southern part of Lake Baikal may be a sensitive area for 24-hour meteorological forecasts of most dust storm events. For the forecast at 1800 UTC on 10 April 2023, the sensitive area becomes much more westerly as well. The large TDE values are arranged from the western side of Inner Mongolia to central Inner Mongolia. Preferentially reducing the errors over the regions in Inner Mongolia may benefit the meteorological forecasts.

From the spatial distributions of CNOP-based sensitive areas presented above, we find that eastern Mongolia, near the city of Ulaanbaatar, is a sensitive area for the 12-hout meteorological forecasts in most dust storms; while the northern parts of Mongolia, closer to the southern parts of Lake Baikal, are sensitive areas for 24-hout meteorological forecasts in most dust storm events.

3.3 | The sensitive area of meteorological fields for dust storm forecasts determined by FSV-type errors

The FSV method is the key method to identify the sensitive areas in operational forecasts and practical target observation field campaigns (Parsons, 2017; Peng & Reynolds, 2006). For each meteorological forecast, the FSV-type error, which includes the same meteorological

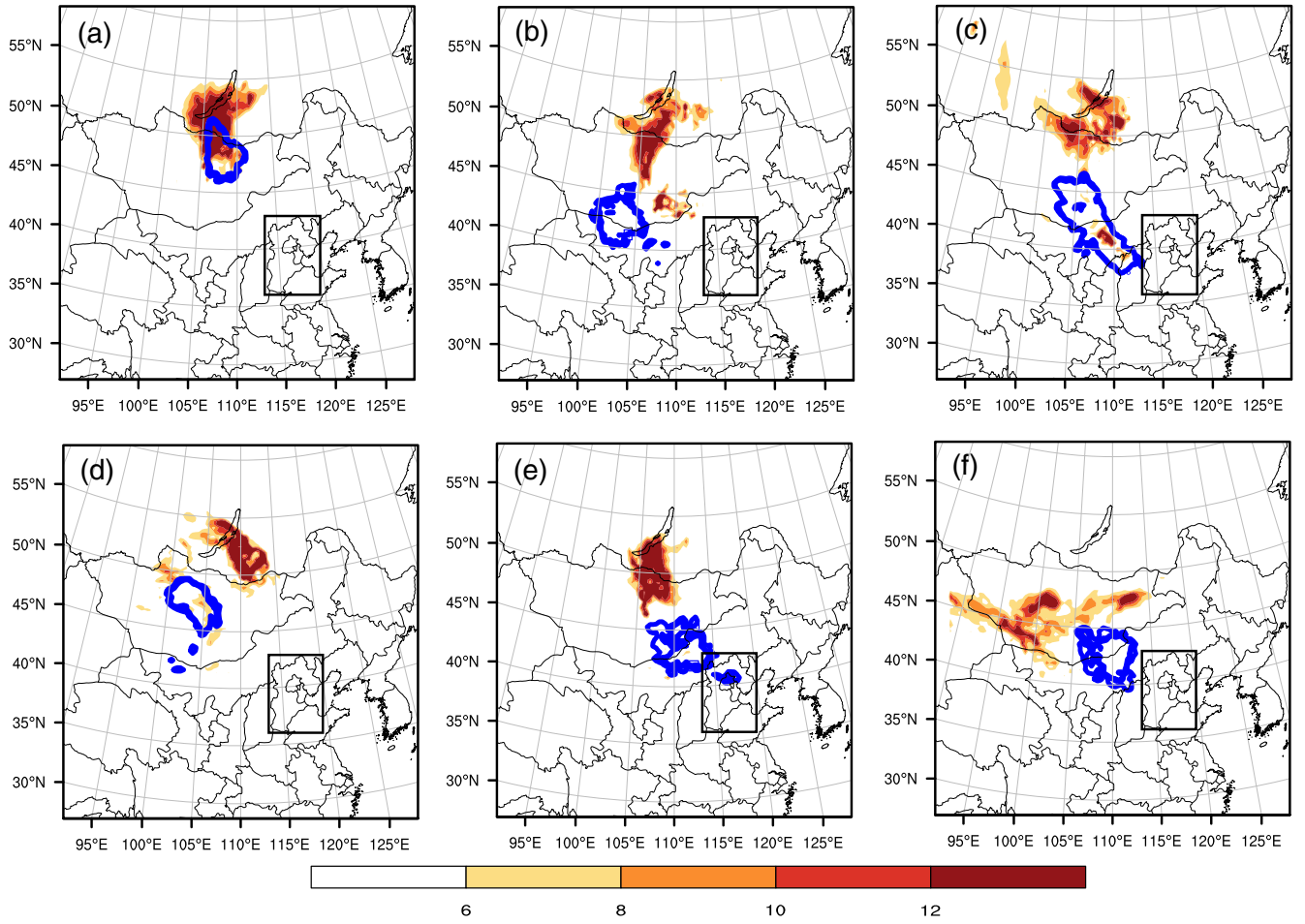

FIGURE 2 The same as Figure 1 but for the 24-hour forecasts. [Colour figure can be viewed at wileyonlinelibrary.com]

variables with the CNOP-type errors, is computed. Similarly, a total of twelve FSV-type errors are obtained and the TDE is also used to measure the comprehensive initial sensitivities. For the 12-hour meteorological forecasts, the FSV-based sensitive areas are to the northwest of BTH as well. However, compared to the CNOP-based sensitive areas, they are much closer to the BTH area, primarily lying in central Inner Mongolia (i.e., Xilingol League), and the northern part of Hebei province. The spatial distances between the CNOP- and FSV-based sensitive areas are case-dependent. For the forecast at 1800 on 10 April 2023, the FSV-based sensitive area exhibits overlap with some parts of the CNOP-based sensitive areas. The spatial distance between the most sensitive grid points identified by the two methods is 189 km. Conversely, for the forecast at 0600 on 28 March 2021, the sensitive areas identified by the two methods are further apart and the most sensitive grid points are 670 km apart.

When the lead time increases from 12 to 24 hours, the FSV-based sensitive areas are distributed further apart from those identified by CNOP-type errors. As we showed earlier, the CNOP-based sensitive areas are mostly located in the southern part of Lake Baikal; however, the FSV-based sensitive areas are much more southern than that. The distributions are also largely dependent on each case. For the cases at 0600 UTC on 22 March 2023 and 1800 UTC on 10 April 2023, the sensitive areas identified by FSV are closer to the northwestern part of the BTH region, while the sensitive areas for the cases at 0600 UTC on 15 March 2021 and 1800 on 10 March 2023 are distributed in the northern part of Mongolia. Western Inner Mongolia is a sensitive area for the remaining two cases. For the forecast at 0600 on 15 March 2021, some parts of the sensitive areas identified by the two methods overlapped. The spatial distance between the two sensitive areas is 263 km. For the other forecasts, the distance range of the sensitive areas identified by the two methods is between 416 km and 819 km, much further than for the 12-hour forecasts.

Till now, we used the CNOP and FSV methods separately to determine the sensitive area of the meteorological field for dust storm forecasts and compared the spatial distributions. We found significant differences in the spatial distribution of the sensitive areas identified by the

two methods. Although they are both distributed in the northwest of BTH, the FSV-based sensitive area is much closer to the BTH region. Theoretically, CNOP can fully account for nonlinear effects, which enables it to provide more accurate sensitive areas. However, in actual forecasts, the effectiveness of CNOP-based sensitive areas in enhancing the accuracy of meteorological forecasts for dust storm events has not yet been numerically validated. Will deploying and assimilating observations on the CNOP sensitive area lead to higher meteorological forecasting skills for dust storm events compared to FSV? This question will be explored in the following section.

4 | THE COMPARISON OF CNOP AND FSV ON IMPROVING THE METEOROLOGICAL FORECAST SKILLS FOR DUST STORM EVENTS

After the sensitive areas are determined separately using the CNOP and FSV methods, we will verify their effectiveness in improving the meteorological forecast skills through numerical experiments. Additionally, we will compare the improvements in meteorological field forecasting resulting from the assimilation of an equal number of observations on the CNOP- and FSV-based sensitive areas, with the aim to offer theoretical suggestions for field campaign implementation.

Specifically, in each forecast, we select the top 50, 100 and 150 grid points with the highest TDE value computed from CNOP-type errors. In this way, three new observation networks are constructed which are determined by CNOP-type errors but with different numbers. Similarly, the observation network determined by FSV-type errors is designed as well. in this way, in each forecast, six observation networks which are determined respectively by CNOP and FSV and various numbers of observations (50, 100, 150) are constructed. As we mentioned in Section 3.1, the "real" observations from these observation networks are assimilated to the control forecast, and if the assimilation forecasts are much closer to the truth, then the effectiveness of sensitive areas will be verified. Moreover, if assimilating the observation networks identified by CNOP-type errors leads to higher improvements than the networks resulting from FSV, then the advantage of CNOP will be verified. The improvement in meteorological forecasts can be quantified by the reduction rates of the composite forecast errors averaged over the concerned vertical levels at the forecast time (AE_V; see Equation 5).

$$R(\sigma) = \iint_{x,y} \frac{1}{2}\left(U^2_{\mathrm{err},\sigma} + V^2_{\mathrm{err},\sigma} + \frac{C_p}{T_r}T^2_{\mathrm{err}}, \sigma\right)dxdy, \tag{7}$$

$$\mathrm{AE_V} = \frac{1}{6}\int_{\sigma} \frac{R_{C,T}(\sigma) - R_{A,T}(\sigma)}{R_{C,T}(\sigma)}d\sigma \times 100\%,$$

$$(\sigma = 1000, 950, 850, 700, 600, 500\ \mathrm{hPa})$$

where $U_{\mathrm{err},\sigma}$, $V_{\mathrm{err},\sigma}$ and $T_{\mathrm{err},\sigma}$ are forecast errors of the zonal, meridional wind and temperature components relative to the observations at layer σ averaged for the BTH region. $R_{C,T}(\sigma)$ measures the composite meteorological forecast errors at the layer σ at the forecast time (T) in the control run; and $R_{A,T}(\sigma)$ measures those forecast errors in the assimilation run. AE_V summarizes the forecast improvements by averaging the error reduction $R(\sigma)$ from the surface to the mid-tropospheric layer at the verification time (T, Equation 6). Positive values of AE_V indicate the improvements of forecast skills in the assimilation run, and larger positive values indicate greater improvements.

The improvements in each forecast when the observations are assimilated, quantified by AE_V are shown in Figure 3. The assimilation of observations on the CNOP-based sensitive areas consistently leads to higher forecast skills, regardless of forecast time. For the 12-hour forecast, assimilating an additional 50 observations on the CNOP-based sensitive areas improves forecast accuracy by 26.37% on average, which is 7.39% higher than assimilating observations on the FSV-based sensitive areas. When the number of observations increases to 100 and 150, the average improvements rise to 27.97% and 31.59% respectively, which are 4.55% and 5.46% higher than the improvements achieved by assimilating observations on the FSV-based sensitive areas. In particular, for the forecast at 0600 UTC on 22 March 2023, assimilating 50 observations in the CNOP-based sensitive area, located on the western side of Mongolia, results in an improvement of 40.87% in forecasting skill. In contrast, assimilating observations within the FSV-based sensitive area, which is mainly concentrated in the northern region of BTH, only leads to a 25.22% improvement in forecasting skill, which is 15.65% lower than the assimilation of obsevations on the CNOP-based sensitive area. Thus, when conducting the target observation field experiments, determination of the sensitive areas is crucial for improving forecasting skill; and the CNOP, which fully accounts for nonlinear effects, is more effective in identifying sensitive areas.

In 24-hour forecasts, the spatial distributions of the sensitive areas identified by the two methods differ significantly, leading to substantial differences in the enhancement of forecasting skill. In general, the assimilation of observations on the CNOP-based sensitive areas has shown advantages compared to those on FSV-based sensitive areas. More specifically, assimilating 50, 100 and 150

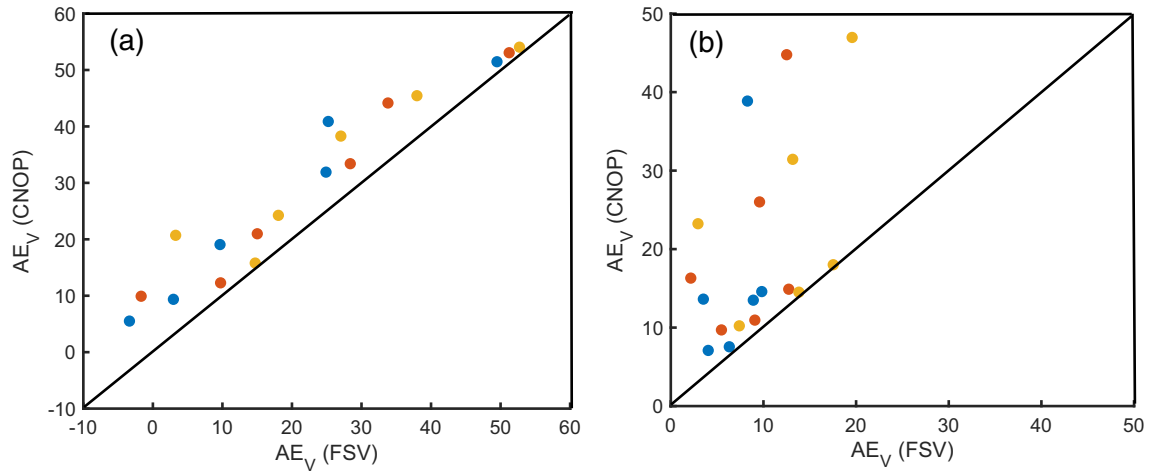

FIGURE 3 Comparison of the forecast improvement quantified by AE_V (forecast errors averaged over the concerned vertical levels) when 50 (blue circles), 100 (red circles) and 150 (yellow circles) grid points are assimilated, for the (a) 12-hour and (b) 24-hour forecasts. [Colour figure can be viewed at wileyonlinelibrary.com]

observations on the CNOP-based sensitive areas will result in a mean improvement of 15.86%, 20.44% and 24.06% quantified by AE_V; while assimilating the same number of observations on the FSV-based sensitive areas leads to improvements of 6.81%, 8.58% and 12.40%. Compared with the 12-hour forecasts, the advantages of CNOP are more apparent for 24-hour forecasts, due to the pronounced nonlinear effects as the forecast time becomes longer. Specifically, for the forecast at 1800 UTC on 10 April 2023, assimilating 50 observations on the CNOP-based sensitive areas lead to an improvement of 38.86%; while if we deploy and assimilate the observations on the FSV-based sensitive areas, which is much closer to the BTH region, the improvement can only reach 8.28%.

By a series of OSEs, we first confirmed the effectiveness of target observation in improving the forecast accuracy of meteorological fields for dust storm events. Moreover, by comparing the forecast improvement achieved by the assimilation of the same number of observations, we demonstrate the advantages of CNOP in identifying sensitive areas, thereby enhancing meteorological forecasts for each dust storm event.

5 | PHYSICAL INTERPRETATIONS

Till now, numerical experiments have shown that deploying observations on the CNOP-based sensitive areas will achieve higher meteorological forecast skills for dust storm events. In this section, we attempt to give physical interpretations of why observations assimilated on the CNOP-based sensitive areas lead to higher forecast results, by comparing the meteorological fields updated with observations assimilated in the CNOP- and FSV-based sensitive areas, respectively. Especially, the meteorological forecast in a super dust storm event which occurred on 22 March 2023 will be introduced in detail. Then we attempt to provide dynamical interpretations on the spatial distribution of the sensitive areas by analyzing the weather patterns.

During 21 and 22 March 2023, due to the strong winds and upstream dust transport, the BTH region experienced a severe dust storm event, and the visibility was only 300–800 m, which has attracted great attention from scientists worldwide (Filonchyk et al., 2024). For the meteorological forecast, the control run shows northerly wind and low-temperature forecast errors in the BTH region, which are likely to impact the transport of dust particles and the accuracy of PM_{10} forecasts. Taking the meteorological fields at 850 hPa as an example, at the initial time (1800 UTC on 21 March), the control run presents significant northerly wind errors and negative temperature errors over eastern Mongolia (Figure 4a). These northerly winds descend, carrying cold air, which results in larger northerly wind and low temperature forecast errors in the northeastern direction of BTH by the forecast time (0600 UTC on 22 March, Figure 4d). Influenced by the forecast errors of cold air in the Jilin and Liaoning provinces, the BTH region also exhibited a northerly wind error of 4.53 $m \cdot s^{-1}$ and a negative temperature error of 2.12°C. When 100 observations on the CNOP-based sensitive areas are assimilated at 12 hours before the forecast time, the assimilation forecast reduces the northerly wind errors and the negative temperature errors on central and eastern Mongolia at the initial time (Figure 4b). The smaller initial errors of wind and temperature in the upstream region in the assimilation run leads to smaller wind and temperature errors downstream, ultimately decreasing the

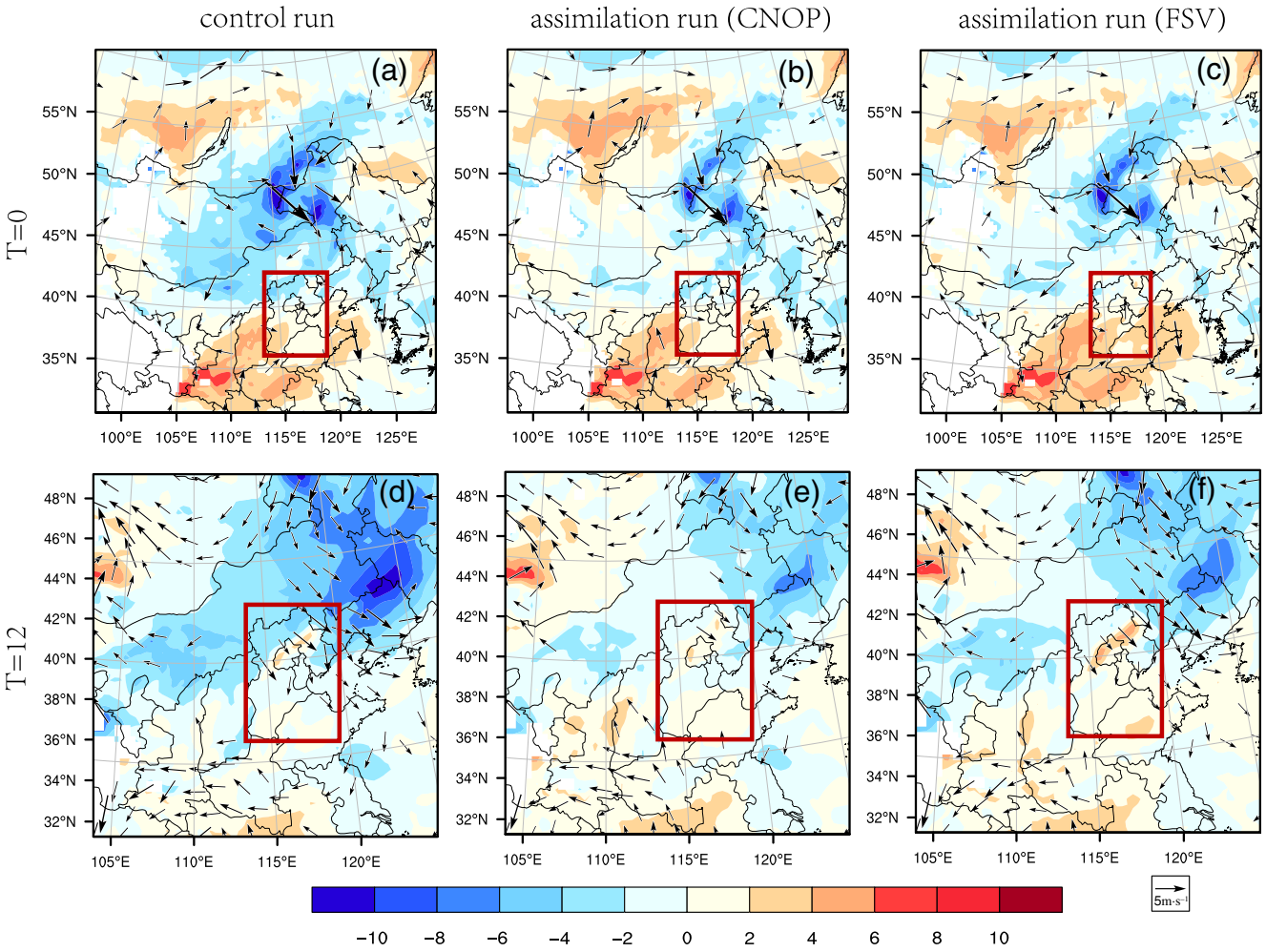

FIGURE 4 The forecast errors in temperature (shaded;°C) and wind (vector; $m \cdot s^{-1}$) at the initial time (top) and the forecast time (bottom) at the 850 hPa level. (a,d) The forecast errors of the control run; (b,d) the forecast errors of the assimilation run when 100 observations on the Conditional Nonlinear Optimal Perturbation (CNOP)-based sensitive area are assimilated; (e,f) the forecast errors of the assimilation run when 100 observations on the First Singular Vector (FSV)-based sensitive area are assimilated. The red rectangle is the Beijing–Tianjin–Hebei (BTH) region. [Colour figure can be viewed at wileyonlinelibrary.com]

northerly wind and low-temperature errors in the BTH region at the forecast time. As a result, the wind forecast error decreases from 4.53 to 3.11 $m \cdot s^{-1}$, and the temperature forecast error decreases from 2.12 to 0.95°C averaged over the BTH region at the forecast time (Figure 4e). By comparison, although the sensitive areas determined by CNOP and FSV are very close and assimilating 100 observations in the FSV-based sensitive areas reduces the initial errors in the eastern part of Mongolia at the initial time (Figure 4c) as well, the reduction is not as extensive. Moreover, the assimilation increases the temperature initial errors in the south of the BTH region, probably due to the imperfect assimilation procedure or the unsolved scales and processes in the model (Janjić et al., 2018). Consequently, although the forecast error in wind field decreases from 4.53 to 4.21 $m \cdot s^{-1}$ and the temperature error decreases from 2.12 to 1.45°C averaged over the BTH region at the forecast time, the assimilation was less effective compared to the assimilation of observations within the CNOP sensitive areas (Figure 4f). When the forecast time increases from 12 to 24 h, the forecast errors in the BTH region primarily originate from northerly wind and cold temperature errors around the southern region of Lake Baikal. Assimilating observations within the CNOP-based sensitive areas helps to mitigate these errors, ultimately reducing the northerly wind error in the downstream BTH region from 5.62 to 5.18 $m \cdot s^{-1}$ and the negative temperature error from 2.83°C to 1.89°C. Additionally, although the objective function (Equation 1) is designed to reduce the forecast errors at the verification time, the assimilation can also enhance the mean forecast performance throughout the forecast period. In contrast, the FSV-based sensitive areas lie much closer to the BTH region. As the model integrates, the assimilation

on these sensitive areas can only reduce the wind error to 5.40 m·s^{-1} and the temperature error to 2.74°C at the forecast time.

We also compare the meteorological forecast errors in other dust storm events. The spatial distributions of forecast errors for each event are presented in Figures S2–S6. Similar to the super storm event, assimilating additional observations on the CNOP-based sensitive areas strengthens or weakens the initial wind fields and modifies the initial temperature fields upstream of the BTH region. As the model integrates, these changes in wind intensity and temperature modify the thermodynamic conditions in the downstream areas, ultimately improving the meteorological forecast skills on the BTH region. To summarize the reduced forecast errors for all the events achieved by the assimilation, we also made a boxplot of forecast errors averaged over the BTH region, for both temperature and wind fields (Figure 5). As shown in Figure 5, assimilating observations on the CNOP-based sensitive areas reduced the mean temperature forecast errors from 3.17 to 2.14°C, while assimilating the same number of observations on FSV-based sensitive areas reduced the forecast errors to 2.59°C. Meanwhile, in wind fields, assimilating observations over the CNOP-based sensitive areas reduced forecast errors from 6.22 to 5.00 m·s^{-1}, compared to 5.47 m·s^{-1} for FSV-based sensitive areas. As to the reasons why the CNOP-based sensitive areas are more effective, these may be related to the effect of the nonlinear advection process, while the FSV is generated in the linearized model and the nonlinear advection process is linearized so that it cannot accurately capture the effect of nonlinear processes. The nonlinear advection process, together with the initial perturbation with the specific structure and environmental fields provided by the control forecast, may contribute to the significant forecast errors in the BTH region. So eliminating the CNOP-type initial errors may result in a larger improvement of forecast skills. Nonetheless, a more in-depth exploration of the underlying dynamical reason is still intended in future research.

In fact, although the distribution of CNOP-based sensitive areas varies for each event, for 24-hour forecasts, they are predominantly located around the southern region of Lake Baikal; while for 12-hour forecasts, they are mostly concentrated in eastern Mongolia. It is widely accepted many strong dust storm events in North China are driven by the Mongolian cyclone system and the associated cold high-pressure center located to its west side (Buhe et al., 2022; Gao et al., 2024; Yin et al., 2022). The significant pressure gradient between the cyclone and the cold high-pressure area enhances northerly surface gusts, which intensify dust emissions in Mongolia and drive the dust particles to the southeast. Concurrently,

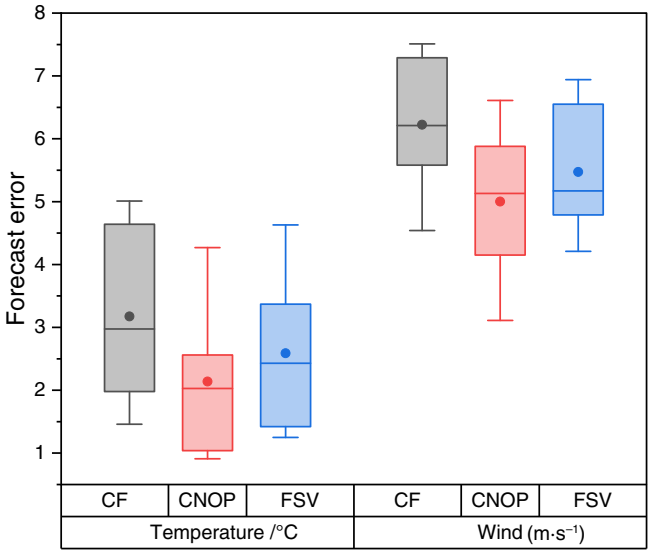

FIGURE 5 Boxplot of the amplitudes of forecast errors of the six events in temperature (°C) and wind (m s^{-1}) averaged over the Beijing–Tianjin–Hebei (BTH) region at the 850 hPa level. The lower and upper box boundaries represent the 25th and 75th percentiles, respectively, while the lines at both ends indicate the minimum and maximum values. The whiskers extend to the values outside the interquartile range (below the 25th percentile and above the 75th percentile). The dots and middle lines represent the mean and median, respectively. CF, Control Forecast; CNOP, the assimilation run when observations on the Conditional Nonlinear Optimal Perturbation (CNOP)-based sensitive area are assimilated; FSV, the assimilation run when the same number of observations on the First Singular Vector (FSV)-based sensitive area are assimilated. [Colour figure can be viewed at wileyonlinelibrary.com]

the ascending motions of Mongolian cyclones lift the dust particles to the troposphere and transport them to North China. The variation in the location and intensity of Mongolian cyclones will affect the coverage and severity of dust storm events in North China (Gui et al., 2022). As demonstrated by Yin et al., 2022, during the period from 2011 to 2021, the strongest Mongolian cyclone happened on 14–15 March 2021, effectively triggering the strongest dust storm in the last decade. The Mongolian cyclone moved eastward, accompanying the eastward progression of the 500 hPa trough during dust storm events. Figure 6 shows the composite 500 hPa geopotential height averaged from six dust storms. Consistent with the previous studies, a deep trough is located on the southern part of southern Lake Baikal 24 hours before the maximum observed PM_{10} concentration over the BTH region (Figure 6a). Then the trough developed and moved southeasterly to the city of Ulaanbaatar 12 hours before the maximum observed PM_{10} concentrations (Figure 6b). Behind the trough, there is a strong cold advection, which leads to the cold air steadily moving to the south. Under the influence of strong cold

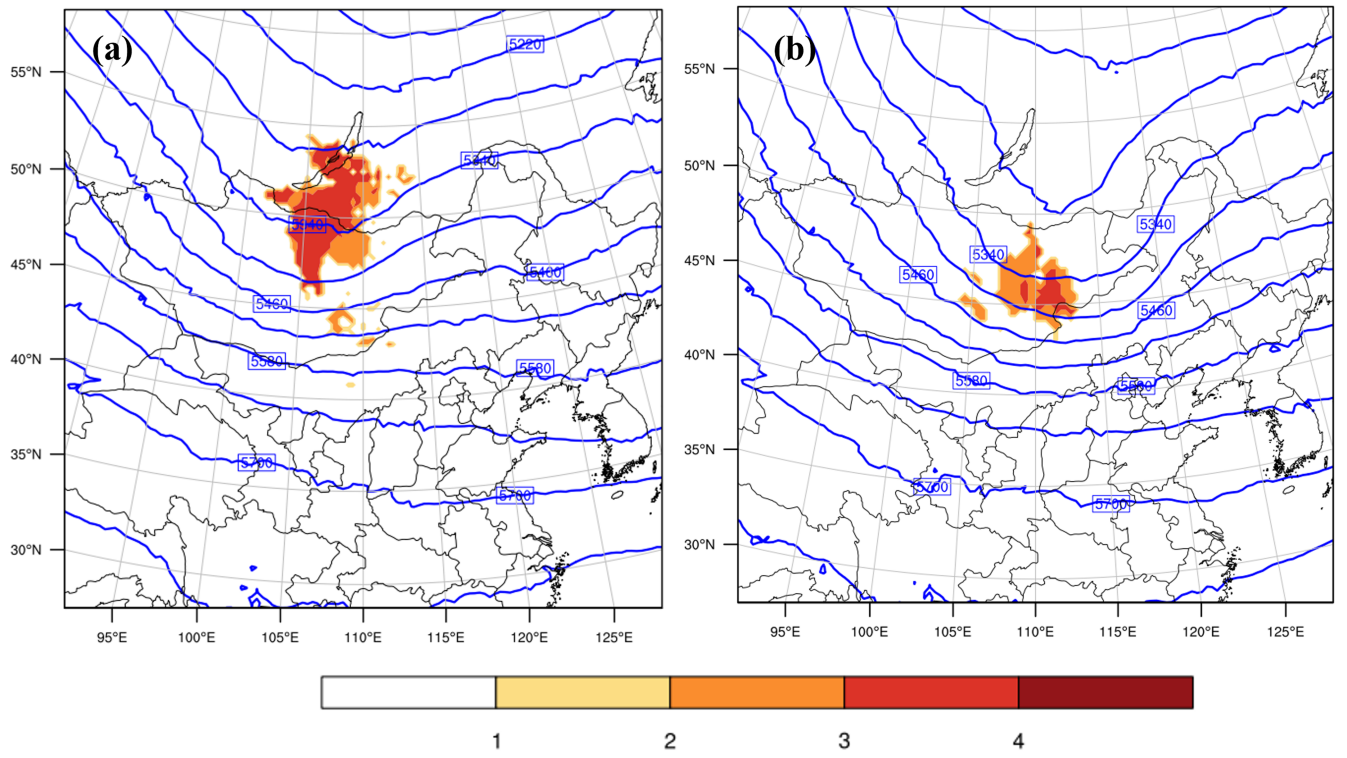

FIGURE 6 The spatial distribution of the 500-hPa geopotential height (contour line) and the distribution of top 100 sensitive grids (shaded) in more than two forecasts. (a) The 24-hour forecast; (b) the 12-hour forecast. [Colour figure can be viewed at wileyonlinelibrary.com]

advection and the passage of a Mongolian cyclone, strong winds swept the sandy areas in Mongolia, transporting surface dust into the upper atmosphere. As the 500-hPa trough moves eastward, the cold high pressure behind the Mongolian cyclone moves eastward, transporting the dust to North China and having great impacts on our country. Meanwhile, if we compare the positions of the sensitive areas and the upper trough, we can find that the sensitive areas of meteorological forecasts with 12- and 24-hour lead times overlapped well with the position of the trough. As the lead time reduces from 24 hours to 12 hours, the sensitive areas move southeasterly from North Mongolia to South Inner Mongolia. That indicates that the meteorological conditions around the upper-level trough are crucial for accurate meteorological forecasts of dust storm events.

So far, we have verified the effectiveness of CNOP-based sensitive areas on improving the meteorological forecasts for dust storm events through numerical experiments; also, we have interpreted the validity by comparing the meteorological forecasts with the assimilation on the CNOP- and FSV-based sensitive areas. Moreover, we try to give dynamical explanations for the general features of sensitive-area distributions of different dust storms. It is therefore expected that the results may provide theoretical guidance for field observations or constructing upper-air radiosonde sites associated with improving dust storm forecasts in the BTH area.

6 | SUMMARY

Dust storms are a frequent meteorological hazard in northern China, characterized by their suddenness and severity. Accurate forecasts of meteorological fields from surface to mid-low troposphere are crucial for dust storm forecasts. However, the current meteorological forecasting capabilities may not be sufficient for providing precise dust storm predictions. To improve the meteorological forecasts for dust storm events, we applied a target observation strategy and investigated the sensitive areas for target observations. By studying six dust storm events in the BTH region from 2021 to 2023, two methods were employed to identify the sensitive areas. The first method, CNOP, fully accounts for nonlinear effects, while the second, FSV, is commonly used in operated forecasts but limited by linear approximations. The sensitive areas identified by the two methods differ significantly, particularly in the 24-hour forecasts. For the forecasts of maximum PM_{10} concentration with a lead time of 24 hours, the CNOP-based sensitive areas are mostly in northern Mongolia, whereas the FSV-based sensitive areas are primarily in southern Mongolia. For the 12-hour forecasts, the CNOP-based sensitive areas are

primarily located in eastern Mongolia, near the city of Ulaanbaatar, whereas the FSV-based sensitive areas lie in central Inner Mongolia.

To numerically validate the role of the identified sensitive areas in improving forecast accuracy, we conducted OSE experiments for each dust storm event. Additionally, we compared the improvements in meteorological forecasts resulting from the assimilation of an equal number of observations in the CNOP-based and FSV-based sensitive areas. Results show that assimilating observations on both the CNOP- and FSV-based sensitive areas improves the meteorological forecast skills for dust storm events in the BTH region. Moreover, the assimilation of observations on the CNOP-based sensitive areas consistently results in higher forecast skills. For the 12-hour forecasts, assimilating 50 observations on the CNOP-based sensitive areas could improve the forecast skill by 26.37% on average, whereas assimilating the same number of observations in the FSV-based sensitive areas results in only a 18.98% improvement. This disparity becomes even more pronounced in the 24-hour forecasts. Assimilating 50 observations on the CNOP-based sensitive areas leads to a 15.68% improvement in forecast skill, whereas doing so in the FSV-based sensitive areas results in only an 6.81% improvement.

After numerically demonstrating the advantages of CNOP, we attempt to give a physical interpretation by comparing the meteorological fields. It is shown that the CNOP method can provide a more accurate identification of the initial errors that contribute to the largest forecast errors in the BTH region. When the observations on the CNOP-based sensitive areas are assimilated, it will reduce the initial wind and temperature errors upstream of the BTH area and then, the modified wind and temperature may modify the thermodynamic field in the downstream areas, finally improving the meteorological forecasts in the BTH region. Moreover, we also find that the location of the sensitive areas overlaps well with the 500-hPa trough, which indicates that the meteorological conditions around the upper-level trough are crucial for accurate meteorological forecasts of the dust storms.

Through numerical experiments and physical interpretations, our study demonstrates that the CNOP method, which fully accounts for nonlinear processes, is more effective in identifying the sensitive areas than the commonly used FSV method. Therefore, for implementing target observation tasks related to dust storms in the BTH region, it is suggested to deploy additional meteorological observations on the sensitive areas identified by the CNOP-type errors to improve the meteorological forecasts of the dust storms. Moreover, since the sensitive areas for 24-hour forecasts are primarily located in northern Mongolia, and for 12-hour forecasts in eastern Mongolia, establishing more upper-air meteorological stations in these regions will be more likely to enhance meteorological forecasts for the BTH region, thus benefiting the forecast skill of dust storm events. As a first attempt to investigate the impact of the nonlinear CNOP method on identifying sensitive areas associated with dust storm forecasts, we concentrate solely on improving the meteorological forecast skills, given their crucial role in dust storm predictions. How the improved meteorological forecasts benefit the dust concentration predictions has not been quantified yet. Thus, further research addressing the impact of target meteorological observations on dust concentration forecasts with the meteorology- and chemistry-coupled model (i.e., WRF-Chem) is expected. Besides, although assimilating observations on the CNOP-based sensitive areas can help enhance the meteorological forecast skills for dust storm events in the BTH region, there are still large differences between the assimilation forecasts and the truth. In this study, we focus solely on the impact of meteorological initial errors on dust storm forecasts and adopt the CNOP or FSV method to eliminate the sensitive meteorological initial errors; however, the model errors can also lead to large forecast errors. To explore the model error effects, Duan and Zhou (2013) proposed a new approach named nonlinear forcing singular vector (NFSV), which represents the total tendency perturbation that describes the combined model errors resulting in the largest forecast errors. To neutralize both the initial and model error effects simultaneously, Duan et al. (2022) formulated an NFSV data assimilation (NFSV-DA) approach. The NFSV-DA considers the combined model errors that come from the model tendency and calculates a tendency perturbation that is superimposed on the model tendency and makes the simulation results closest to the observation. The practical outcome of this approach is to offset the effect of initial and model errors simultaneously through NFSV-DA. Till now, the NFSV-DA approach has been successfully applied in ENSO predictions and is verified being effective in forecasting the type of El-Nino events (Tao et al., 2020; Zheng et al., 2023). Therefore, it is expected that neutralizing the effects of both initial and model errors through appropriate approaches, such as NFSV-DA, with meteorological forecast models, such as the WRF model, will further help achieve higher forecast skills of meteorological forecasts and the ensuing dust concentration forecasts. Furthermore, besides the meteorological fields, dust concentrations are also a key input for dust storm forecasts. With the continuous advancement of observation technologies and the improvement of collaborative observation network construction, massive, high-quality multisource dust particle data can be easily assessed. How to effectively integrate these observational data and assimilating both dust particle and meteorological data into numerical

models to optimize dust storm forecasting accuracy may also be a key issue for future research.

Beside target observation technique, ensemble forecast is also an effective strategy to improve the numerical forecast skills of dust storms (Singh et al., 2021; Kim et al., 2023). In fact, both target observation and ensemble forecast utilize the sensitivity of initial perturbations to improve the forecast skills. In the present study on target observation, we show that the CNOP-type error can effectively represent the optimally growing initial perturbation in the nonlinear model and preferentially eliminating by data assimilation the meteorological initial error on which CNOP focuses can help enhance the forecast skills significantly. Considering the sensitivity of these optimally growing initial perturbations, it conceivable that, when they are applied to the ensemble forecasting, they would certainly enhance the forecasting skills. In fact, these optimally growing initial perturbations are the orthogonal CNOPs proposed by Duan and Huo (2016); and the orthogonal CNOPs have been applied in tropical cyclone (TC) track ensemble forecasts, significantly improving their forecasting skills. Especially for unusual TC tracks, such as the sharp northward-turning track of TC Megi (2010) and the counterclockwise loop track of TC Tembin (2012), the ensemble members generated by the orthogonal CNOPs can successfully reproduce these, while the forecasts made by SVs, bred vectors and random perturbations fail to do so (Zhang et al., 2023). Thus, it is expected that orthogonal CNOPs can be used in dust storm ensemble forecasts in the near future and contribute to enhance the forecasting skills of dust storms.

ACKNOWLEDGEMENTS

This research is supported by the National Key R&D Program of China (Grant No. 2023YFC3705501), National Natural Science Foundation of China (No. 42475064) and the R&D Program of Beijing Municipal Education Commission (No. KM202410028014). The numerical simulation was supported by the National Key Scientific and Technological Infrastructure project "Earth System Numerical Simulation Facility" (EarthLab). The authors sincerely appreciate the three anonymous reviewers for their constructive comments, which greatly enhanced the overall quality of the paper.

CONFLICT OF INTEREST STATEMENT

The contact author has declared that none of the authors has any competing interests.

DATA AVAILABILITY STATEMENT

The data that support the findings of this study are available from the corresponding author upon reasonable request.

ORCID

Wansuo Duan https://orcid.org/0000-0002-0122-2794

REFERENCES

An, L.C., Zhang, H.D., Gui, H.L. & Zhang, T.H. (2018) Analysis of a sand and dust weather process affecting North China and Huanghuai in spring 2015. *Meteorological Monthly*, 44(1), 180–188.

Bao, Y.S., Zhu, L.H., Guan, L., Guan, Y.H. et al. (2019) Assessing the impact of Chinese FY-3/MERSI AOD data assimilation on air quality forecasts: sand dust events in northeast China. *Atmospheric Environment*, 205, 78–89.

Bauer, P., Thorpe, A. & Brunet, G. (2015) The quiet revolution of numerical weather prediction. *Nature*, 525, 47–55.

Bei, N., Wu, J., Elser, M., Feng, T., Cao, J., El-Haddad, I. et al. (2017) Impacts of meteorological uncertainties on the haze formation in Beijing–Tianjin–Hebei (BTH) during wintertime: a case study. *Atmospheric Chemistry and Physics*, 17,14579–14591.

Birgin, E.G., Martinez, J.M. & Raydan, M. (2001) Algorithm 813: SPG – software for convex-constrained optimization. *ACM Transactions on Mathematical Software*, 27, 340–349.

Buhe, C.L., Zhuge, A.R., Xie, Z.W., Yong, M. & Purevjav, G. (2022) The development of a powerful Mongolian cyclone on 14–15 march 2021: Eddy energy analysis. *Atmospheric and Oceanic Science Letters*, 15, 100259.

Chan, K.L., Wiegner, M., Flentje, H., Mattis, I., Wagner, F., Gasteiger, J. et al. (2018) Evaluation of ECMWF-IFS (version 41R1) operational model forecasts of aerosol transport by using ceilometer network measurements. *Geoscientific Model Development*, 11, 3807–3831.

Chen, D.K., Smith, N. & Kessler, W. (2018) The evolving ENSO observing system. *National Science Review*, 5, 805–807.

Chen, S.Y., Du, S., Bi, H., Zhao, D., Zhang, Y., Chen, Y. et al. (2024) Review on identification and forecasting of dusty weather. *Journal of Desert Research*, 44(1), 11–21.

Chen, S.Y., Zhao, D., Huang, J., He, J., Chen, Y., Chen, J. et al. (2023) Mongolia contributed more than 42% of the dust concentrations in northern China in march and April 2023. *Advances in Atmospheric Sciences*, 40(9), 1549–1557.

Duan, H.X., Li, Y.H., Huo, W., Qin, H. & Ma, Y.F. (2016) Objective verification of GRAPES_SDM model in Xinjiang, China. *Journal of Desert Research*, 36(2), 441–448.

Duan, W.S., Feng, R., Yang, L.C. & Jiang, L. (2022) A new approach to data assimilation for numerical weather forecasting and climate prediction. *Journal of Applied Analysis and Computation*, 12(3), 1007–1021.

Duan, W.S. & Huo, Z.H. (2016) An approach to generating mutually independent initial perturbations for ensemble forecasts: orthogonal conditional nonlinear optimal perturbations. *Journal of the Atmospheric Sciences*, 73, 997–1014.

Duan, W.S., Yang, L.C., Mu, M., Wang, B., Shen, X.S. et al. (2023) Recent advances in China on the predictability of weather and climate. *Advances in Atmospheric Science*, 40(8), 1521–1547.

Duan, W.S. & Zhou, F.F. (2013) Nonlinear forcing singular vector of a two-dimensional quasi-geostrophic model. *Tellus A: Dynamic Meteorology and Oceanography*, 65(1), 18452.

Dudhia, J. (1989) Numerical study of convection observation during the winter monsoon experiment using a mesoscale two-dimensional model, J. Atmos. *Sci.*, 46, 3077–3107.

Feng, J., Qin, X., Wu, C., Zhang, P., Yang, L., Shen, X.S. et al. (2022) Improving typhoon predictions by assimilating the retrieval of atmospheric temperature profiles from the FengYun-4A's geostationary interferometric infrared sounder (GIIRS). *Atmospheric Research*, 280, 106391.

Feng, T.C., Yuan, T.G., Cao, J.H., Wang, Z.K., Zhi, R., Hu, Z.Y. et al. (2023) The influence of dust on extreme precipitation at a large city in North China. *Science of the Total Environment*, 901, 165890.

Filonchyk, M., Peterson, M., Zhang, L.F. & Yan, H.W. (2024) An analysis of air pollution associated with the 2023 sand and dust storms over China: aerosol properties and PM10 variability. *Geoscience Frontiers*, 15(2), 101762.

Ganor, E., Stupp, A., Osetinsky, I. & Alpert, P. (2010) Synoptic classification of lower troposphere profiles for dust days. *Journal of Geophysical Research*, 115, D11201.

Gao, J., Ding, T. & Gao, H. (2024) Dominant circulation pattern and moving path of the Mongolian cyclone for the severe sand and dust storm in China. *Atmospheric Research*, 301, 107272.

Gholami, H., Mohamadifar, A. & Collins, A.L. (2020) Spatial mapping of the provenance of storm dust: application of data mining and ensemble modelling. *Atmospheric Research*, 233, 104716.

Gong, S.L. & Zhang, X.Y. (2008) CUACE/dust – an integrated system of observation and modeling systems for operational dust forecasting in Asia. *Atmospheric Chemistry and Physics*, 8, 2333–2340.

Goris, N. & Elbern, H. (2015) Singular vector-based targeted observations of chemical constituents: description and first application of the EURAD-IM-SVA v1.0. *Geoscientific Model Development*, 8, 3929–3945.

Gui, K., Che, H., Yao, W., Zheng, Y. et al. (2023) Quantifying the contribution of local drivers to observed weakening of spring dust storm frequency over northern China (1982–2017). *Science of the Total Environment*, 894, 164923.

Gui, K., Yao, W., Che, H., An, L., Zheng, Y., Li, L. et al. (2022) Record-breaking dust loading during two mega dust storm events over northern China in march 2021: aerosol optical and radiative properties and meteorological drivers. *Atmospheric Chemistry and Physics*, 22, 7905–7932.

Hersbach, H., Bell, B., Berrisford, P. et al. (2020) The ERA5 global reanalysis. *Quarterly Journal of the Royal Meteorological Society*, 146, 1999–2049.

Hong, S.Y., Ying, N. & Dudhia, J. (2006) A new vertical diffusion package with an explicit treatment of entrainment processes. *Monthly Weather Review*, 134, 2318–2341.

Hu, J.Y. & Duan, W.S. (2016) Relationship between optimal precursory disturbances and optimally growing initial errors associated with ENSO events: implications to target observations for ENSO prediction. *Journal of Geophysical Research – Oceans*, 121, 011386.

Iacono, M.J., Delamere, J.S., Mlawer, E.J., Shephard, M.W., Clough, S.A. & Collins, W.D. (2008) Radiative forcing by long-lived greenhouse gases: calculations with the AER radiative transfer models. *Journal of Geophysical Research-Atmospheres*, 113, D13103.

Janjić, T., Bormann, N., Bocquet, M. et al. (2018) On the representation error in data assimilation. *Quarterly Journal of the Royal Meteorological Society*, 144, 1257–1278.

Jiang, L., Duan, W.S. & Liu, H.L. (2022) The most sensitive initial error of sea surface height anomaly forecasts and its implication for target observations of mesoscale eddies. *Journal of Physical Oceanography*, 52, 723–740.

Joly, A., Jorgensen, D., Shapiro, M.A., Thorpe, A., Bessemoulin, P. et al. (1997) The fronts and Atlantic storm-track experiment (FASTEX): scientific objectives and experimental design. *Bulletin of the American Meteorological Society*, 78, 1917–1940.

Kaimian, F., Li, Q., Wu, C. et al. (2019) Evaluation of different machine learning approaches to forecasting PM2.5 mass concentrations. *Aerosol and Air Quality Research*, 19, 1400–1410.

Kalnay, E. (2002) *Atmospheric modeling, data assimilation and predictability*. Cambridge: Cambridge University Press.

Kim, M., Cho, J.H. & Ryoo, S.-B. (2023) Development and assessment of ADAM3 ensemble prediction system. *Scientific Online Letters on the Atmosphere*, 19, 26–32.

Knippertz, P. & Todd, M.C. (2012) Mineral dust aerosols over the Sahara: meteorological controls on emission and transport and implications for modeling. *Reviews of Geophysics*, 50, RG1007.

Leith, C.E. (1974) Theoretical skill of Monte Carlo forecasts. *Monthly Weather Review*, 102, 409–418.

Lin, C., Wang, Z. & Zhu, J. (2008) An ensemble Kalman filter for severe dust storm data assimilation over China. *Atmospheric Chemistry and Physics*, 8, 2975–2983.

Lin, C., Zhu, J. & Wang, Z.F. (2009) Uncertainty analysis of a dust-transport model. *Chinese Journal of Atmospheric Sciences (in Chinese)*, 33(2), 232–240.

Lin, Y.L., Farley, R.D. & Orville, H.D. (1983) Bulk parameterization of the snow field in a cloud model, Clim appl. *Meteorologie*, 22, 1065–1092.

Lorenz, E.N. (1963) Deterministic nonperiodic flow. *Journal of the Atmospheric Sciences*, 20, 130–141.

Lorenz, E.N. (1975) *Climate predictability. The Physical Basis of Climate and Climate Modeling, Global Atmospheric Research Programme Publication Series, No.16*. Geneva: World Meteorology Organization, pp. 132–136.

Majumdar, S.J. (2016) A review of targeted observations. *Bulletin of the American Meteorological Society*, 97, 2287–2303.

Majumdar, S.J., Aberson, S., Bishop, C.H. et al. (2011) *Targeted observations for improving numerical weather prediction: An overview*, Vol. 15. Geneva: World Weather Research Programme/THORPEX Publication.

Mee Kim, H., Kyung Kay, J. & Jung, B. (2008) Application of adjoint-based forecast sensitivities to Asian dust transport events in Korea. *Water, Air, and Soil Pollution*, 195, 335–343.

Mee Kim, H., Kyung Kay, J., Yang, E.G., Kim, S. & Lee, M. (2013) Statistical adjoint sensitivity distributions of meteorological forecast errors of Asian dust transport events in Korea. *Tellus B: Chemical and Physical Meteorology*, 65(1), 20554.

Mu, M., Duan, W.S., Chen, D.K. & Yu, W.D. (2015) Target observations for improving initialization of high-impact ocean-atmospheric environmental events forecasting. *National Science Review*, 2, 226–236.

Mu, M., Duan, W.S. & Wang, B. (2003) Conditional nonlinear optimal perturbation and its applications. *Nonlinear Processes in Geophysics*, 10, 493–501.

Parsons, D.B., Beland, M., Burridge, D., Bougeault, P., Brunet, G. et al. (2017) THORPEX research and the science of prediction. *Bulletin of the American Meteorological Society*, 98, 807–830.

Peng, M.S. & Reynolds, C.A. (2006) Sensitivity of tropical cyclone forecasts as revealed by singular vectors. *Journal of the Atmospheric Sciences*, 63, 2508–2528.

Piao, J., Chen, W., Wei, K., Cai, Q., Zhu, X. & Du, Z. (2023) Increased sandstorm frequency in North China in 2023: climate change reflection on the Mongolian plateau. *Innovations*, 4(5), 100497.

Qian, Z.A., Cai, Y., Liu, J.T., Liu, C.M., Li, D.L. & Song, M.H. (2006) Some advances in dust storm research over China-Mongolia areas. *Chinese Journal of Geophysics*, 49(1), 83–92.

Qin, X.H., Duan, W.S., Pak, W.C., Chen, B.Y. & Kang-Ning, H. (2023) Effects of dropsonde data in field campaigns on forecasts of tropical cyclones over the western North Pacific in 2020 and role of CNOP sensitivity. *Advances in Atmospheric Sciences*, 40, 791–803.

Sarafian, R., Nissenbaum, D., Raveh-Rubin, S. et al. (2023) Deep multi-task learning for early warnings of dust events implemented for the Middle East. *Npj Climate and Atmospheric Science*, 6, 23.

Shao, Y., Klose, M. & Wyrwoll, K.-H. (2013) Recent global dust trend and connections to climate forcing. *Journal of Geophysical Research – Atmospheres*, 118, 11107–11118.

Singh, C., Singh, S.K., Chauhan, P. & Budakoti, S. (2021) Simulation of an extreme dust episode using WRF-CHEM based on optimal ensemble approach. *Atmospheric Research*, 249, 105296.

Slingo, J. & Palmer, T. (2011) Uncertainty in weather and climate prediction. *Philosophical Transactions of the Royal Society A*, 369, 4751–4767.

Snyder, C. (1996) Summary of an informal workshop on adaptive observations and FASTEX. *Bulletin of the American Meteorological Society*, 77, 953–961.

Talagrand, O. (1997) Assimilation of observations, an introduction. *Journal of the Meteorological Society of Japan, Series II*, 75, 191–209.

Tao, L.J., Duan, W.S. & Vannitsem, S. (2020) Improving forecasts of El Niño diversity: a nonlinear forcing singular vector approach. *Climate Dynamics*, 55, 739–754.

Toth, Z. & Kalnay, E. (1997) Ensemble forecast at NCEP and the breeding method. *Monthly Weather Review*, 125, 3297–3319.

Ukhov, A., Ahmadov, R., Grell, G. & Stenchikov, G. (2021) Improving dust simulations in WRF-Chem v4.1.3 coupled with the GOCART aerosol module. *Geoscientific Model Development*, 14, 473–493.

Vova, O., Kappas, M., Renchin, T. & Degener, J. (2015) Land degradation assessment in Gobi-Altai province. In: *Proc. of the trans-Discplinary research conference: building resilience of Mongolian rangelands*. Ulaanbaatar, Mongolia, 9–10 June 2015.

Yang, E., Kim, H.M., Kim, J. & Kay, J.K. (2014) Effect of observation network design on meteorological forecasts of Asian dust events. *Monthly Weather Review*, 142, 4679–4695.

Yang, L.C., Duan, W.S. & Wang, Z.F. (2023) An approach to refining the ground meteorological observation stations for improving PM2.5 forecasts in Beijing-Tianjin-Hebei region. *Geoscientific Model Development*, 16, 3827–3848.

Yang, L.C., Duan, W.S., Wang, Z.F. & Yang, W.Y. (2022) Toward targeted observations of the meteorological initial state for improving the PM2.5 forecast of a heavy haze event that occurred in the Beijing-Tianjin-Hebei region. *Atmospheric Chemistry and Physics*, 22, 11429–11453.

Yin, Z.C., Wan, Y., Zhang, Y.J. & Wang, H.J. (2022) Why super sandstorm 2021 in North China. *National Science Review*, 9, nwab165.

Yu, Y., Mu, M., Duan, W. & Gong, T. (2012) Contribution of the location and spatial pattern of initial error to uncertainties in El Niño predictions. *Journal of Geophysical Research*, 117, C06018.

Zhang, H., Duan, W. & Zhang, Y. (2023) Using the orthogonal conditional nonlinear optimal perturbations approach to address the uncertainties of tropical cyclone track forecasts generated by the WRF model. *Weather Forecasting*, 38, 1907–1933.

Zhang, H.S. & Li, X.L. (2014) Review of the field measurements and parameterization for dust emission during sand-dust events. *Acta Meteorologica Sinica*, 72(5), 987–1000.

Zhang, K., Mu, M., Wang, Q., Yin, B. & Liu, S. (2019a) CNOP-based adaptive observation network designed for improving upstream Kuroshio transport prediction. *Journal of Geophysical Research: Oceans*, 124, 4350–4364.

Zhang, X.X., Sharratt, B., Lei, J.Q., Wu, C.L., Zhang, J., Zhao, C. et al. (2019b) Parameterization schemes on dust deposition in northwest China: model validation and implications for the global dust cycle. *Atmospheric Environment*, 209, 1–13.

Zhang, Z.H. & Huisingh, D. (2018) Combating desertification in China: monitoring, control, management and revegetation. *Journal of Cleaner Production*, 182, 765–775.

Zheng, Y.C., Duan, W.S., Tao, L.J. & Ma, J.J. (2023) Using an ensemble nonlinear forcing singular vector data assimilation approach to address the ENSO forecast uncertainties caused by the "spring predictability barrier" and El Niño diversity. *Climate Dynamics*, 61, 4971–4989.

Zhu, J., Lin, C.Y. & Wang, Z.F. (2009) Dust storm ensemble forecast experiments in East Asia. *Advances in Atmospheric Sciences*, 26(6), 1053–1070.

SUPPORTING INFORMATION

Additional supporting information can be found online in the Supporting Information section at the end of this article.

How to cite this article: Yang, L. & Duan, W. (2025) Sensitive areas for target observation associated with meteorological forecasts for dust storm events in the Beijing–Tianjin–Hebei region. *Quarterly Journal of the Royal Meteorological Society*, e4975. Available from: https://doi.org/10.1002/qj.4975